XVI International Conference on Computational Plasticity. Fundamentals and Applications
COMPLAS 2021
E. Oñate, D. Peric, M. Chiumenti and Eduardo de Souza Neto (Eds)

DYNAMIC ANALYSIS OF THE DISSIPATIVE RESPONSE OF INTERVERTEBRAL DISCS ABOUT A NONLINEAR PRESTRESSED STATE

J.-B. GARCHER*, L. ROULEAU* AND J.-F. DEÜ*

* Structural Mechanics and Coupled Systems Laboratory
Conservatoire national des arts et métiers
292 rue Saint-Martin, 75003 Paris, France
web page: www.lmssc.cnam.fr/

Key words: Biomechanics, Intervertebral disc, Dynamic response, Hyperelasticity, Finite element model

Abstract. Due to their critical location in the human anatomy, intervertebral discs (IVD) are subject to complex loading conditions. Experimental and numerical studies on intervertebral discs under static loading are widely analysed in the literature, giving insight into the mechanical characteristics of IVD. Nevertheless, due to complex experimental protocols and challenging simulations, their dynamic behaviour is scarcely studied. Further studies are necessary to better understand the mechanisms in degenerative disc disease and support the design of robust disc prothesis. The goal of this work is to examine the nonlinear effects of time-dependent loading on the mechanical response of IVD, through numerical simulations.

A finite element model which accounts for the complexity of the IVD (heterogeneity, fiber anisotropy, hyperelasticity, viscoelasticity) is developed. The hyperelastic Holzapfel-Gasser-Ogden (HGO) material model was implemented to describe the nonlinear behaviour of the annulus fibrosus and the dissipative behaviour of the fibers is also considered through a finite strain viscoelasticity model.

Vibrations about a nonlinear prestressed state will be considered to model physiological dynamic loading such as whole body vibration. A complementary aspect focuses on the viscoelastic behaviour of the IVD, by quantifying the dissipated energy through hysteresis loops. The influence of inputs parameters (preload, strain-rate and excitation frequency) on the dynamic responses will be also analysed.

1 INTRODUCTION

Low back pain is a common problem that will affect most people in their life. Degenerative disc disease (DDD) is a medical condition in which a damaged spinal disc causes pain. In general, causes of spine pathology are multifactorial, but the 21st century way of life may lead to accelerated anatomic changes and an early loss of function of the intervertebral disc (IVD). The mechanisms behind DDD are still unclear, especially the relationship between external loads and disc damage. The IVD plays a major role in

the normal mechanical function of the spine : it is the principal joint between two vertebrae and it allows the three-dimensional mobility of the spine (torsion, flexion and lateral bending). The IVD also acts as a shock absorber within the spine that is particularly important in daily activities.

The IVD consists of two components :

- the nucleus pulposus (NP), the central gelatinous material. It has an important water content and a high deformable isotropic behaviour. It represents about 50% of the IVD

- the annulus fibrosus (AF), a multilayer structure around the NP. Several concentric lamellas composed of collagen fibers constitute a high stiffness structure which keeps the NP inside the IVD.

The mechanical response of the IVD is governed by the composition and structural organization of its components. The interaction between these two components leads to a reliable function of the IVD, and the whole IVD's behaviour is jeopardized if one of them is degenerative (due for instance to the dehydration of the NP or a lack of stiffness of the AF). Some experimental analysis are reported on both human and animal IVDs [7] and highlight the influence of external loading (loading rate, strain rate) and physical parameters (age, spinal level, anatomy) on DDD. However, experimental studies are very challenging due to the large influence of testing environment and sample preconditioning. In particular, in vivo boundary conditions are hardly reproducible in a testing environment. Therefore, numerical models are necessary to better understand mechanisms behind degenerative disc disease. The flexibility of numerical models, based on material properties obtained experimentally, offers a great possibility to apply complex static or time-dependent boundary conditions.

This study is devoted to the nonlinear and dissipative simulation of the IVD about a prestress state. The IVD is preloaded by the mass of the upper body creating an internal pressure inside the NP. The nonlinear behaviour of the IVD to static loading is reported in literature on experimental tests and numerical simulations. But the dynamic behaviour about this preloaded state, is still little known. Through this study, we explore the relationship between external loads and dynamic disc properties. Such studies could be a modern database in the development of disc prothesis, aiming at designing reliable disc replacement and providing the required individual treatment.

The first section focuses on the specific constitutive model for the AF, a fiber-reinforced viscoelastic structure. Then, a finite element model of a lumbar L4/5 IVD is described, integrating the material model implemented for the AF. Various computational simulations are finally presented in Section 3 to describe the behaviour of IVD for different loading scenarios.

2 ANISOTROPIC VISCOELASTIC MODEL FOR ANNULUS FIBROSUS

In this section, the specific material law implemented for the AF in the finite element model is presented. A hyperelastic large deformation formulation is used to define the

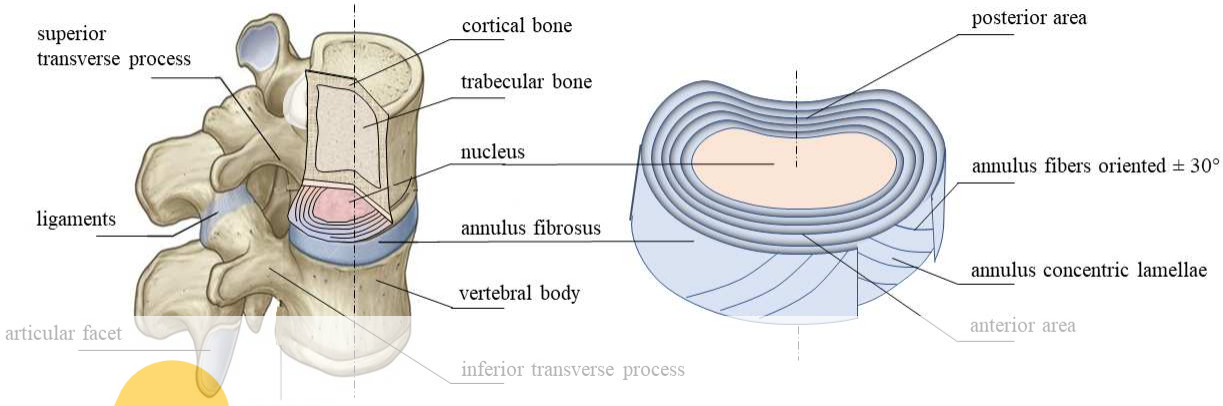

Figure 1: Main functional spinal unit composition.

nonlinear behaviour of the IVD. The Holzapfel-Gasser-Ogden (HGO) material model was implemented to represent the mechanical contribution of collagen fibers, and its viscous behaviour is also taken into account via a finite strain viscoelastic formulation [2]. The main features of this model are presented here.

The position vector of a particle is denoted $\mathbf{X}$ in the reference configuration Ω_0 (at t=0), and $\mathbf{x}(\mathbf{X},t)$ in the current configuration Ω after transformation. A Lagrangian description is used, with Ω_0 as reference configuration.

2.1 Hyperelasticity framework for fiber-reinforced composite

The deformation gradient is defined as $\mathbf{F}(\mathbf{X},t) = \partial\mathbf{x}(\mathbf{X},t)/\partial\mathbf{X}$. We also introduce the right Cauchy-Green tensor $\mathbf{C} = \mathbf{F}^T\mathbf{F}$ and the Green-Lagrange strain tensor $\mathbf{E} = 0.5(\mathbf{C}-\mathbf{1})$. The volume ratio is defined as the jacobian determinant of the transformation $J(\mathbf{X},t) = \det(\mathbf{F}(\mathbf{X},t)) > 0$. The deformation of biological tissues are classically splitted into a volumetric (spherical) part and an isochoric (deviatoric) part. This decomposition can be applied to both $\mathbf{F}$ and $\mathbf{C}$ tensors. We classically denote $\bar{\mathbf{F}}$ and $\bar{\mathbf{C}}$ the isochoric transformation tensors and $\mathbf{F}_v$ and $\mathbf{C}_v$ the volumetric transformation tensors. This decomposition leads to $\mathbf{F} = \bar{\mathbf{F}}\mathbf{F}_v$ and $\det(\bar{\mathbf{F}}) = 1$ while $\det(\mathbf{F}_v) = J(\mathbf{X},t)$. This development can be extended to the Cauchy-Green tensor $\mathbf{C}$, so that we may write the isochoric deformation tensor as:

$$\bar{\mathbf{C}} = J(\mathbf{X},t)^{-\frac{2}{3}}\mathbf{C} \tag{1}$$

The anisotropic structure of the AF requires the definition of two unit vector fields $\mathbf{a}_1^0(\mathbf{X})$ and $\mathbf{a}_2^0(\mathbf{X})$ characterizing the fiber direction at point $\mathbf{X}$ in the reference configuration Ω_0. The action of the deformation gradient on $\mathbf{a}_1^0(\mathbf{X})$ and $\mathbf{a}_2^0(\mathbf{X})$ defines the stretch of the fiber

$$\lambda_{a_1}\mathbf{a}_1(\mathbf{x},t) = \mathbf{F}(\mathbf{X},t)\mathbf{a}_1^0(\mathbf{X}), \qquad \lambda_{a_2}\mathbf{a}_2(\mathbf{x},t) = \mathbf{F}(\mathbf{X},t)\mathbf{a}_2^0(\mathbf{X}) \tag{2}$$

where λ_{ai} $(i = 1,2)$ is the fiber stretch along the direction $\mathbf{a}_i^0$. As fiber directions $\mathbf{a}_i(\mathbf{x},t)$

are unit vector fields, is it possible to express the square of each fiber stretch as $(\lambda_{a_i})^2 = \mathbf{C} : \mathbf{A}_i^0$, where $\mathbf{A}_i^0 = \mathbf{a}_i^0 \otimes \mathbf{a}_i^0$ $(i = 1, 2)$ define the structural tensor of family fibers. Through hyperelastic continuum theory, a strain energy density W is defined by derivating the stress-strain relationships. For fiber reinforced composites, this strain energy density can be decomposed into an isochoric part $W_{iso}(\bar{\mathbf{C}}, \mathbf{A}_1^0, \mathbf{A}_2^0)$, itself separable into fiber (index f) and matrix (index m) components $W_{iso,f}(\bar{\mathbf{C}}, \mathbf{A}_1^0, \mathbf{A}_2^0)$ and $W_{iso,m}(\bar{\mathbf{C}})$, and an volumetric part $W_{vol}(\mathbf{J})$

$$\begin{aligned} W &= W_{iso,m}(\bar{\mathbf{C}}) + W_{iso,f}(\bar{\mathbf{C}}, \mathbf{A}_1^0, \mathbf{A}_2^0) + W_{vol}(\mathbf{J}) \\ &= c_1(\bar{I}_1 - 3) + c_2(\bar{I}_2 - 3) + \frac{k_1}{2k_2}\left(e^{k_2(\bar{I}_4-1)^2} + e^{k_2(\bar{I}_6-1)^2} - 2\right) + k_0(1-J)^2 \end{aligned} \tag{3}$$

where $\bar{I}_1$, $\bar{I}_2$, $\bar{I}_4$ and $\bar{I}_6$ are modified invariants associated to the tensors $\bar{\mathbf{C}}$, $\mathbf{A}_1^0$ and $\mathbf{A}_2^0$. We can identify in this expression the matrix contribution governed by $\bar{I}_1$ and $\bar{I}_2$, and the fiber contributions governed by $\bar{I}_4$ and $\bar{I}_6$. The fibers cannot be subjected to compression, so we consider $W_{iso,f}(\bar{\mathbf{C}}, \mathbf{A}_1^0, \mathbf{A}_2^0)$ only for $\bar{I}_4 \geq 1$ and $\bar{I}_6 \geq 1$. Then, the hyperelasticity theory from a lagrangian point of view links the second Piola-Kirchhoff stress tensor $\mathbf{S}$ to the energy density by:

$$\mathbf{S} = 2\frac{\partial W}{\partial \mathbf{C}} = \mathbf{S}_{iso,m} + \mathbf{S}_{iso,f} + \mathbf{S}_{vol} \tag{4}$$

where $\mathbf{S}_{iso,m}$ (resp. $\mathbf{S}_{iso,f}$) is derived from $W_{iso,m}$ (resp. $W_{iso,f}$). They represent stress tensors associated to the isochoric transformation. Similarly, $\mathbf{S}_{vol}$ derived from W_{vol} represents the stress tensor associated to the volumetric transformation.

2.2 Addition of a viscoelastic contribution

In order to introduce a viscoelastic contribution in the model, we define $\mathbf{Q}_\alpha$, $\alpha = 1, .., N$, internal variables of isochoric stresses coming from the Clausius-Planck inequality [2]. We split each isochoric stress tensor into an equilibrium part, denoted by the ∞ symbol, and non-equilibrium parts:

$$\mathbf{S} = (\mathbf{S}_{iso,m}^{\infty} + \sum_{\alpha=1}^{N} \mathbf{Q}_{\alpha,m}) + (\mathbf{S}_{iso,f}^{\infty} + \sum_{\alpha=1}^{N} \mathbf{Q}_{\alpha,f}) + \mathbf{S}_{vol} \tag{5}$$

A generalization of the 1D linear Maxwell model to the three-dimensional and nonlinear problem is used to describe the evolution of each internal variable. In Eq.(5), N represents the number of viscous branches considered in the viscoelastic model and $\mathbf{Q}_\alpha$ is the internal stress of the α^{th} branch. The equations governing the evolution of each internal variable $\mathbf{Q}_\alpha$ $(\alpha = 1, ..., N)$ are:

$$\dot{\mathbf{Q}}_{\alpha,m} + \frac{\mathbf{Q}_{\alpha,m}}{\tau_{\alpha,m}} = \beta_{\alpha,m}\dot{\mathbf{S}}_{iso,m}^{\infty}, \qquad \dot{\mathbf{Q}}_{\alpha,f} + \frac{\mathbf{Q}_{\alpha,f}}{\tau_{\alpha,f}} = \beta_{\alpha,f}\dot{\mathbf{S}}_{iso,f}^{\infty} \tag{6}$$

The initial configuration is set as $\mathbf{Q}_{\alpha,m}(t=0)=\mathbf{0}$ and $\mathbf{Q}_{\alpha,m}(t=0)=\mathbf{0}$. Couple of viscous parameters $\tau_{\alpha,m}$ and $\beta_{\alpha,m}$ (resp. $\tau_{\alpha,f}$ and $\beta_{\alpha,f}$) are introduced for each α^{th} matrix (resp. fibers) branch as relaxation time and energy factor parameters.

We consider a time interval $t\in[0,T]$ with time discretization characterized by $\Delta t = t_{n+1}-t_n$. The evaluation of each quantity at time t_n is denoted by the index n (e.g. $\mathbf{S}(t_n)=\mathbf{S}|_n$). For numerical implementation, Eq.(6) is expressed as convolution integrals, which can be discredized by a mid-point method to obtain the recurrence update formula for $\mathbf{Q}_{\alpha,m}|_{n+1}$ and $\mathbf{Q}_{\alpha,f}|_{n+1}$. For $\mathbf{Q}_{\alpha,m}$, the recurrence update formula is:

$$\mathbf{Q}_{\alpha,m}|_{n+1}=\mathbf{H}_{\alpha,m}|_n+\beta_{\alpha,m}e^{-\Delta t/2\tau_{\alpha,m}}(\mathbf{S}^{\infty}_{iso,m}|_{n+1}) \tag{7}$$

where the matrix history term is defined as:

$$\mathbf{H}_{\alpha,m}|_n=e^{-\Delta t/2\tau_{\alpha,m}}\left(e^{-\Delta t/2\tau_{\alpha,m}}(\mathbf{Q}_{\alpha,m}|_n)-\beta_{\alpha,m}(\mathbf{S}^{\infty}_{iso,m}|_n)\right) \tag{8}$$

Similar equations can be derived for the fiber contribution.
The constitutive model above is implemented in a finite element method framework. Since the hyperelastic formulation required a Newton-Raphson procedure, the elasticity tensor (tangent moduli) is calculated at each Newton-Raphson iteration. For time-dependant simulations, a Newmark integration scheme is used.

2.3 Numerical example on representative volume element of AF

In order to clearly understand the physical mechanisms of the constitutive model, a small representative volume of the AF is considered, meshed by a single 20-node hexahedron element. We focus on the relative influence of the viscoelastic contribution of the matrix and the fibers. Four cases are studied, as illustrated in figure 2. For simplicity sake, only one Maxwell branch is considered for the fibers and the matrix ($N=1$ in Eq.(5)).

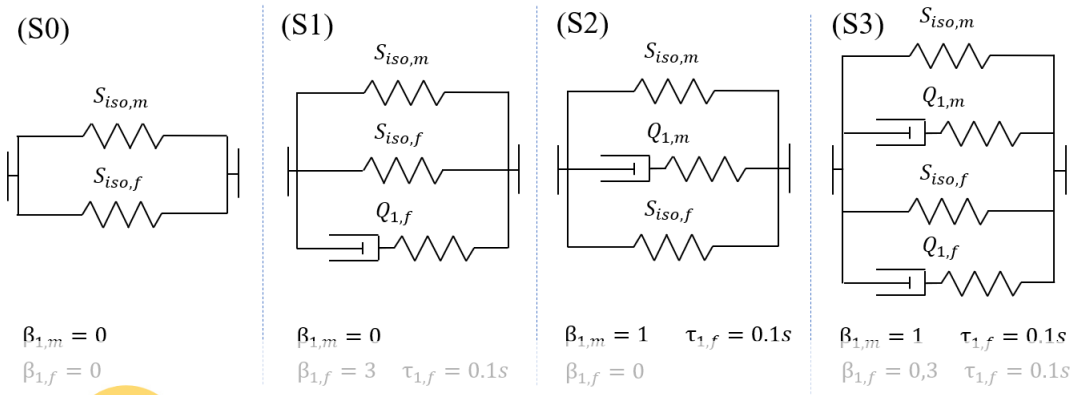

Figure 2: A rheological interpretation of isochoric contribution of the AF. Four cases are studied: (S0) without viscoelastic contribution, (S1) with only fibers viscoelastic contribution, (S2) with only matrix viscoelastic contribution, (S3) with viscoelastic contribution on both matrix and the fibers

Planar symmetric boundary conditions are applied to three faces of the cube while a time-dependent pressure $P(t) = 1 \cdot \sin(5 \cdot t)$ MPa is applied on the upper face (see figure 3, left). Fibers orientations are defined by an angular parameter $\alpha = 30°$. Hyperelastic parameters are set to $k_1 = 1$ MPa and $k_2 = 200$ for fibers and to $c_1 = 0.25$ MPa and $c_2 = 0$ MPa for the matrix part. A compressible material is considered with a Poisson's ratio $\nu = 0.45$, and k_0 is defined as $k_0 = (c_1 + c_2)/(1 - 2\nu)$.

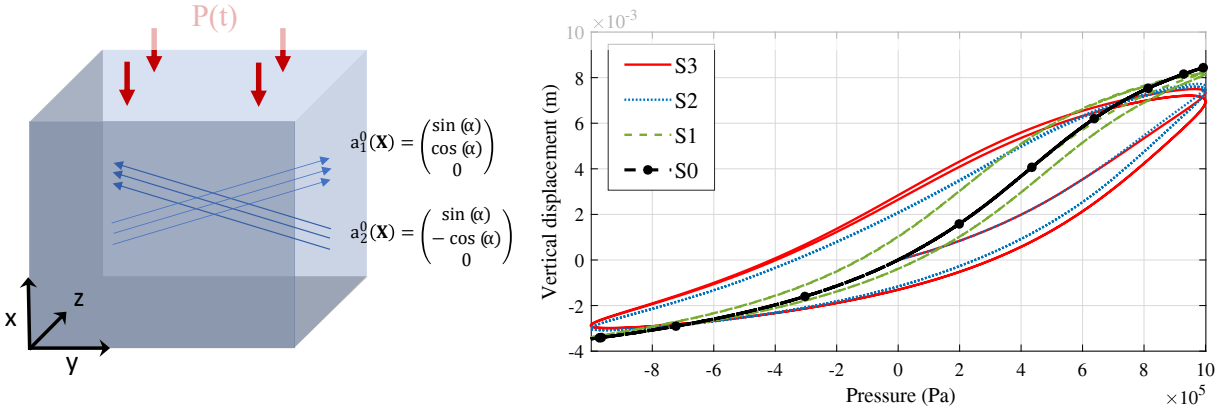

Figure 3: Representative volume element of the AF (left) and hysteresis curves for the four studied cases (right).

The analysis of the upper displacement shows a hysteresis phenomenon. The first study (S0) highlights the nonlinear static behaviour in tension and compression. The stiffness of the representative volume element is higher in compression. This is likely due to the contribution associated to the volumetric transformation (S_{vol}) that is more important in compression than in traction. Figure 3 shows that the dissipated behaviour is widely

dependent on the source of the viscoelastic contribution. The fibers contribute relatively more than the matrix to the dissipated energy of the AF representative volume element in a load cycle.

3 SIMULATION ON PRELOAD LUMBAR DISC

In this section, we are interested in the dynamic behaviour of the IVD under several loading scenarios. To that purpose, a finite element model of a lumbar L4/L5 IVD is developed and both quasi-static and dynamic simulation are carried out.

3.1 Geometry, materials and preloading

The IVD geometry considered in this study (figure 4, left) represents a lumbar disc L4/5, and has been defined from parametric equations describing the AF and NP profiles [6]. The AF is defined by the HGO strain energy density (Eq.(3)) while the NP is defined by the Mooney-Rivlin strain energy density :

$$W^{NP} = W^{NP}_{iso} + W^{NP}_{vol} = c_{1,N}(\bar{I}_1 - 3) + c_{2,N}(\bar{I}_2 - 3) + k_{0,N}(1 - J)^2 \tag{9}$$

A viscoelasticity contribution is added on the isochoric part via a generalized Maxwell model, as described in Section 2.2, for the NP and the AF (fibers and matrix). For the AF, the same values of viscoelastic parameters are taken for the fibers and the matrix: $\tau_{1,m} = \tau_{1,f} = \tau_{1,A}$ and $\beta_{1,m} = \beta_{1,f} = \beta_{1,A}$. All parameters are extracted from the literature and result from curve fitting experimental data. The material properties considered for the AF and the NP are listed in Tables 1 and 2. The constitutive equations have been implemented in Comsol Multiphysics.

$c_{1,A}$ (Mpa)	$c_{2,A}$ (Mpa)	$k_{0,A}$ (Mpa)	k_1 (Mpa)	k_2	$\tau_{1,A}$ (s)	$\beta_{1,A}$
0.25	0	5e6	1e6	200	0.1	1

Table 1: Material parameters of the HGO model and the generalized Maxwell model (1 branch) for the AF (data from [1]).

$c_{1,N}$ (Mpa)	$c_{2,N}$ (Mpa)	$k_{0,N}$ (Mpa)	$\tau_{1,N}$ (s)	$\beta_{1,N}$	$\tau_{2,N}$ (s)	$\beta_{2,N}$	$\tau_{3,N}$ (s)	$\beta_{3,N}$
0.12	0.03	15e6	0.042	0.500	0.051	0.199	6.000	0.132

Table 2: Material parameters of the Mooney-Rivlin model and the generalized Maxwell model (3 branches) for the NP.

Figure 4 illustrates the various loading scenarios considered in this study. The loading scenarios (A), (B) and (C) correspond to static/quasi-static simulations (no inertial effects) while the loading scenarios (D) and (E) are associated to dynamic simulations.

In simulations (A) and (C), a static load is uniformly applied to the upper face of the IVD. This load represents the upper body weight which is classically comprised between 400 N and 650 N. In this work, we consider an preload $F = 600$ N.
In simulations (B), (C) and (E), a time-dependent loading is applied to the upper face of the IVD. In this work, we focus on harmonic loading $f(t) = P_0 \cos(2\pi\ f\ t)$ (with $P_0 = 0.25$ MPa). In the quasi-static simulations (B) and (C), the inertial effects are neglected contrary to the dynamic simulation (E).
The dynamic simulations (D) and (E) consider linear vibrations about a prestress state corresponding to the application of the upper body weight. The mass of the IVD is negligible compared to the mass of the upper body mass so that the oscillatory mass in simulations (D) and (E) is the upper body mass $M = 60$ kg (the mass density of the AF and the NP are not defined in the model).

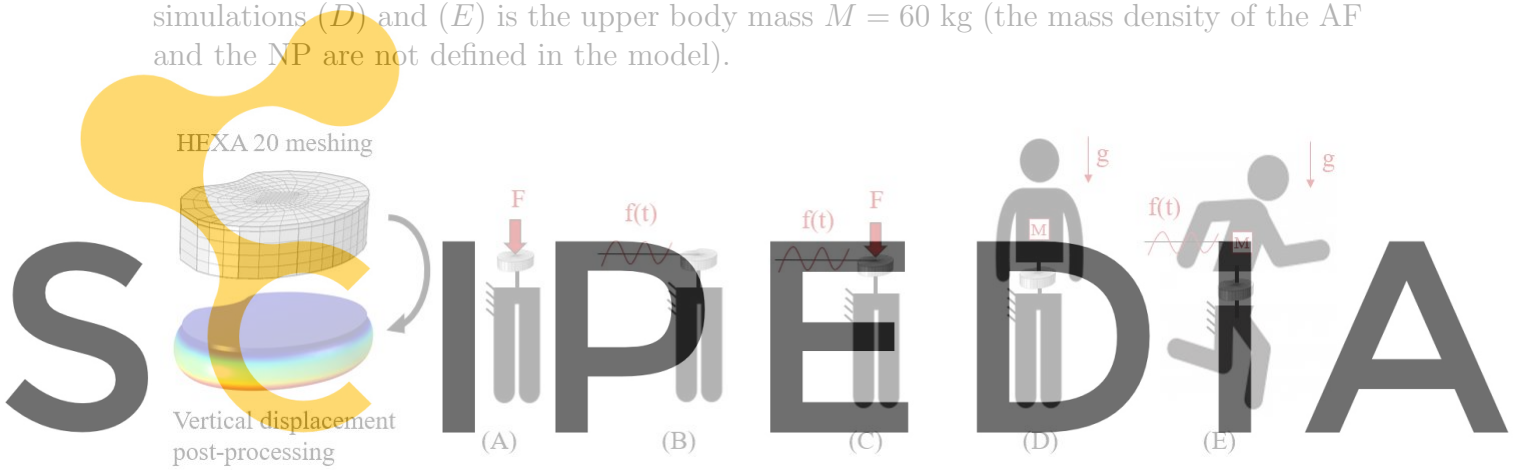

Figure 4: Geometry of IVD and post-processing mapping (left) and boundary conditions apply on the upper side of L4/5 IVD (right).

3.2 Results

The finite element model was validated under static conditions (A) with experimental results from the literature. When post-processing the results of the other simulations, we focus on the vertical displacement of one node of the upper face. The left-hand side of Digure 5 evidences a nonlinear hardening behaviour of the IVD. Results of simulations (B) and (C) show that for a given strain rate (here $f = 0.5$ Hz), the dissipated energy in a load cycle is lower if the static preload is applied. The right-hand side of Figure 5 illustrates the influence of the quasi-static loading strain rate on the nonlinear an dissipative behaviour of the IVD. An increasing strain rate produces a weaker hardening behaviour and reduces the energy dissipated in a cycle. Further studies will be conducted to quantify accurately the dissipated energy.

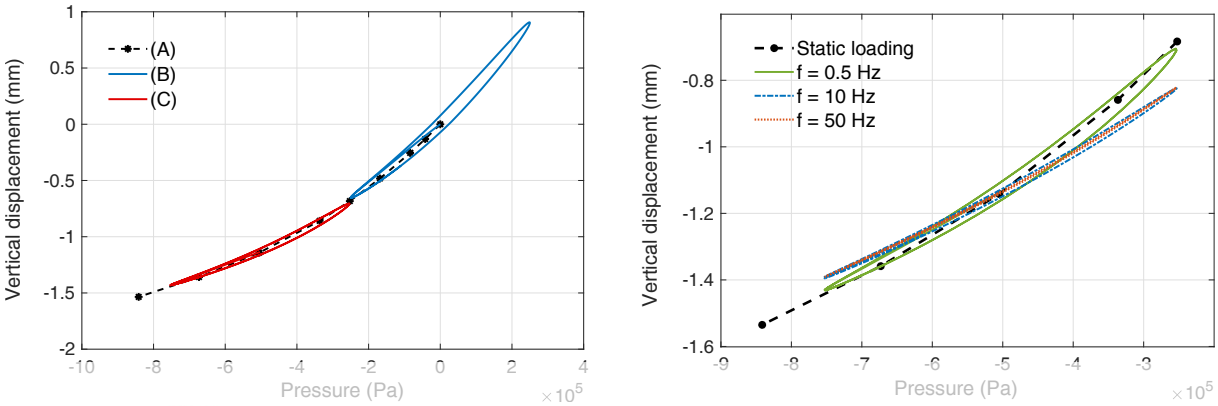

Figure 5: Quasi-static analysis (A), (B) and (C) (right). Influence of the quasi-static loading strain rate on the nonlinear an dissipative behaviour of the IVD.

To better understand the dynamic behaviour of the IVD, modal analysis are first carried out (*D*). Experimental studies are usually concerned with the first tension-compression mode and resonant frequencies ranging from 9 Hz to 30 Hz are reported in the literature for an oscillating mass $M = 40$ kg [3, 5]. The resonant frequency computed is in good agreement with the experiments (see figure 6). Figure 6 compares the resonant frequency of the first tension-compression mode with and without a static preload (linear vibrations about a nonlinear prestress state) for sereval values of upper body mass. The increase of stiffness due to the nonlinearity of the IVD affects significantly the resonant frequency (about 25% increase for $M = 40$ kg).

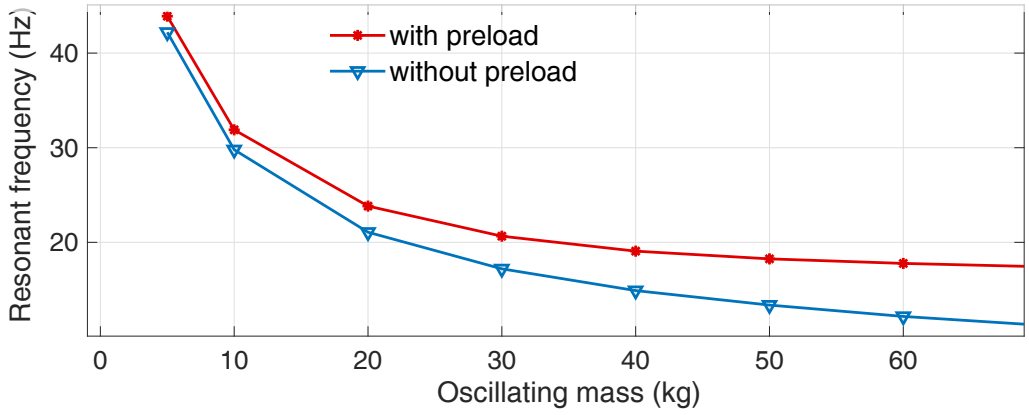

Figure 6: Modal analysis (D): influence of the oscillating mass and static preload on the resonant frequency of the first tension-compression mode of the IVD.

Finally, dynamic simulations are performed in the time-domain to study the linear response of the IVD about a nonlinear prestress state. An upper body mass of $M = 60$ kg is considered for the application of the static preload and the frequency of the harmonic

load varies from 5 Hz to 30 Hz. Larger amplitudes are observed in Figure 7 near the resonant frequency at 18 Hz, as predicted by the modal analysis with preload. The IVD's dynamic response is computed with and without the viscoelastic contribution of the AF and the NP. Figure 7 indicates that the dissipated energy in the IVD due to the viscoelastic behaviour of the AF and the NP causes a significant reduction of the amplitude's response near the resonance frequency. This viscoelastic effect becomes negligible at 5 Hz and 30 Hz.

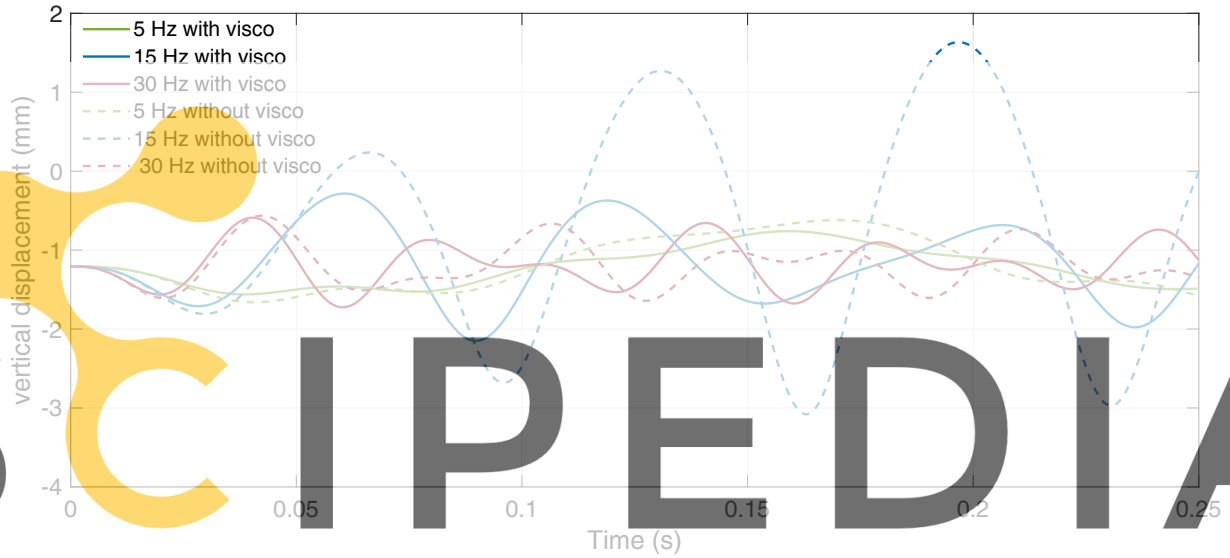

Figure 7: Dynamic analysis (F). Influence of the excitation frequency and of the viscoelastic contribution.

4 CONCLUSION

A finite element model of a L4/5 lumbar IVD has been presented. A hyperelastic model combine with a generalised Maxwell model adapter to the finite strain theroy has been considered for both the AF and the NP. The hyperelastic model implemented for the AF, the HGO model, was chosen to respect the anisotropic structure of fiber-reinforced tissues. Preliminary simulations were performed to validate the model by comparison with experimental values reported in the literature, and to better understand to role of the AF and the NP in the nonlinear and dissipative behaviour of the IVD. Further studies will be carried out to quantify accurately the dissipated energy.

Some numerical aspects are still challenging in this finite element framework, such as the treatment of incompressiblity. Note that the Poisson's ratio of the AF is about $\nu = 0.45$, which can be numerically treated as any compressible material by a penalty method with the coefficient k_0. However, the NP is considered as a nearly-incompressible material ($\nu = 0.49$), so a mixed-formulation is used for the whole IVD simulation. Although displacement fields are less sensitive to the Poisson's ratio than the pressure/stress, other ways of treating the material incompressiblity could be implemented in order to limit numerical errors [4].

The multiple phenomena observable at organ scale show the complexity to predict the dynamic response of IVD. Future work will focus on parametric studies in order to identify the most prevalent parameters in behaviour changes. Due to the large range of global parameters, a patient-specific work could be an interesting approach to set some parameters related to the IVD's geometry or the mass of upper body for instance. A model order reduction based on the previous model could be used to propose individual treatment for DDD.

References

[1] R. Eberlein, G. A. Holzapfel, and C. A. J. Schulze-Bauer. "An anisotropic model for annulus tissue and enhanced finite element analyses of intact lumbar disc bodies". In: *Computer Methods in Biomechanics and Biomedical Engineering* 4 (2001), pp. 209–229.

[2] G. A. Holzapfel and T. C. Gasser. "A viscoelastic model for fiber-reinforced composites at finite strains: Continuum basis, computational aspects and applications". In: *Comput. Methods Appl. Mech. Engrg.* (2001).

[3] O. Izambert et al. "Dynamic stiffness and damping of human intervertebral disc using axial oscillatory displacement under a free mass system". In: *European Spine Journal* (2003).

[4] C. Kadapa and M. Hossain. "A linearised consistent mixed displacement pressure formulation for hyperelasticity". In: *arXiv : 2004.13201* (2020).

[5] M. Kasra, A. Shirazi-Adl, and G. Drouin. "Dynamics of human lumbar intervertebral joints. Experimental and finite-element investigations". In: *Spine* (1992).

[6] J. Paige Little, M. J. Pearcy, and G. J. Pettet. "Parametric equations to represent the profile of the human intervertebral disc in the transverse plane". In: *Medical & Biological Engineering & Computing* 45 (2007), pp. 939–945.

[7] N. Newell et al. "Biomechanics of the human intervertebral disc: a review of testing techniques and results". In: *Journal of the Mechanical Behavior of Biomedical Materials* 69 (2017), pp. 420–434.